Ambuguity of Ultrashort Pulses Retrieved From the Intensity Autocorrelation and Power Spectrum Traces

J. –H. Chung, A.M. Weiner

Center for Education and Research in
Information Assurance and Security

&

School of Electrical and Computer Engineering
Purdue University, West Lafayette, IN 47907

Ambiguity of Ultrashort Pulse Shapes Retrieved From the Intensity Autocorrelation and the Power Spectrum

Jung-Ho Chung, *Student Member, IEEE,* and Andrew M. Weiner, *Fellow, IEEE*

Abstract—We construct several examples of distinct asymmetric–symmetric pulse pairs with identical or essentially identical intensity autocorrelations and power spectra. From these examples, we infer that pulse retrieval methods based on these two data sets alone produce ambiguous solutions. Furthermore, we used the constructed pulse pairs as test cases to assess the degree of difference in the corresponding interferometric autocorrelations. In several cases, we found that the differences in the interferometric autocorrelations are sufficiently small that they might be quite challenging to distinguish in a practical experimental context.

Index Terms—Ambiguity, interferometric autocorrelation, phase retrieval, pulse reconstruction, retrieval algorithm, ultrafast pulse measurement.

I. INTRODUCTION

BECAUSE of the difficulty in resolving temporal shapes of optical pulses on a femtosecond scale using relatively slow electronic detectors, many techniques to indirectly determine the ultrashort pulse shape have been developed [1]–[8], [10], [11]. Frequency-resolved optical gating (FROG) is one of the most commonly used measurement methods [1]. The measurement provides a two-dimensional data set in the time-frequency domain, which is usually sufficient for unique reconstruction of the amplitude and phase of the ultrashort pulse via iterative phase retrieval algorithms. Other techniques, such as the spectral phase interferometry for direct electric field reconstruction (SPIDER) [2], the spectrally and temporally resolved upconversion technique (STRUT) [3], and the direct optical spectral phase measurement (DOSPM) [4], permit direct determination of the amplitude and phase without using iterative techniques, provided certain assumptions are satisfied experimentally.

On the other hand, there has been a long-standing interest in pulse characterization using easy-to-implement correlation techniques [5]. However, the simplest of these measurements are not sufficient to uniquely determine the pulse shape. For example, detecting the output power from a linear Michelson interferometer produces the electric field autocorrelation. This

Fig. 1. The schematic of Case I, where the phase of an assumed asymmetric pulse is specified and the phase of the symmetric pulse is retrieved.

is equivalent to using a spectrometer to measure the power spectrum, which is the Fourier transform of the electric field autocorrelation. Thus, the pulse shape cannot be retrieved, since the spectral phase information is lost. Likewise, it has long been accepted that the intensity autocorrelation function contains insufficient information to obtain the pulse shape. Interferometric autocorrelation functions have also been widely utilized for pulse characterization [6]; however, they have never been demonstrated to be sufficient for unique pulse shape reconstruction.

Combining such one-dimensional data sets, however, can give the capability for uniquely characterizing the pulse amplitude and phase. Since this approach has advantages over two-dimensional measurements including the FROG method, such as less complex experimental setups and faster convergence of retrieval algorithms, several researchers have investigated pulse reconstruction methods based on one-dimensional data sets [7], [8], [10], [11]. Naganuma *et al.* combined as the input to their iterative algorithm the interferometric and electric field autocorrelation functions [7], which correspond to three one-dimensional data sets, namely, the intensity autocorrelation, the second harmonic field autocorrelation, and the power spectrum.
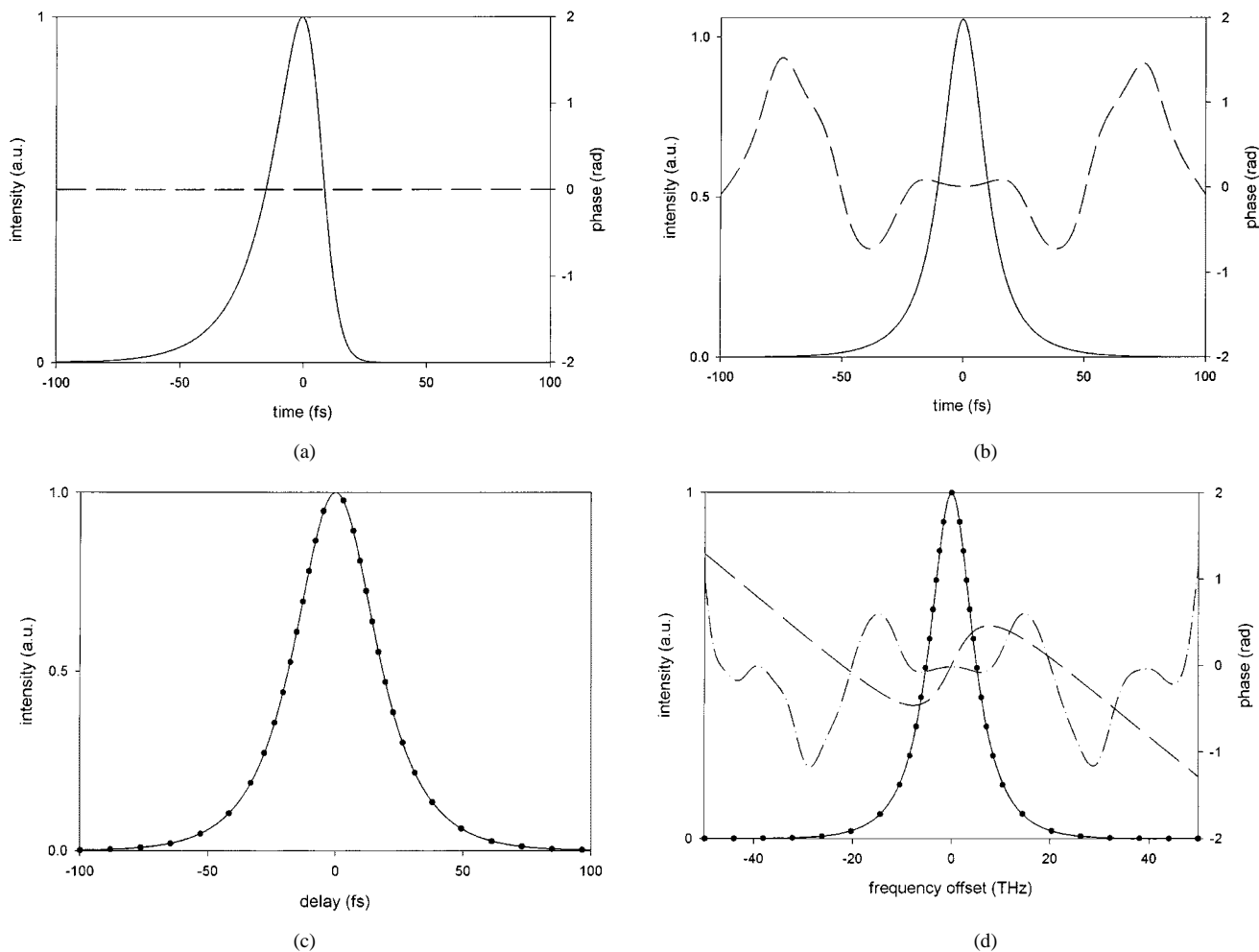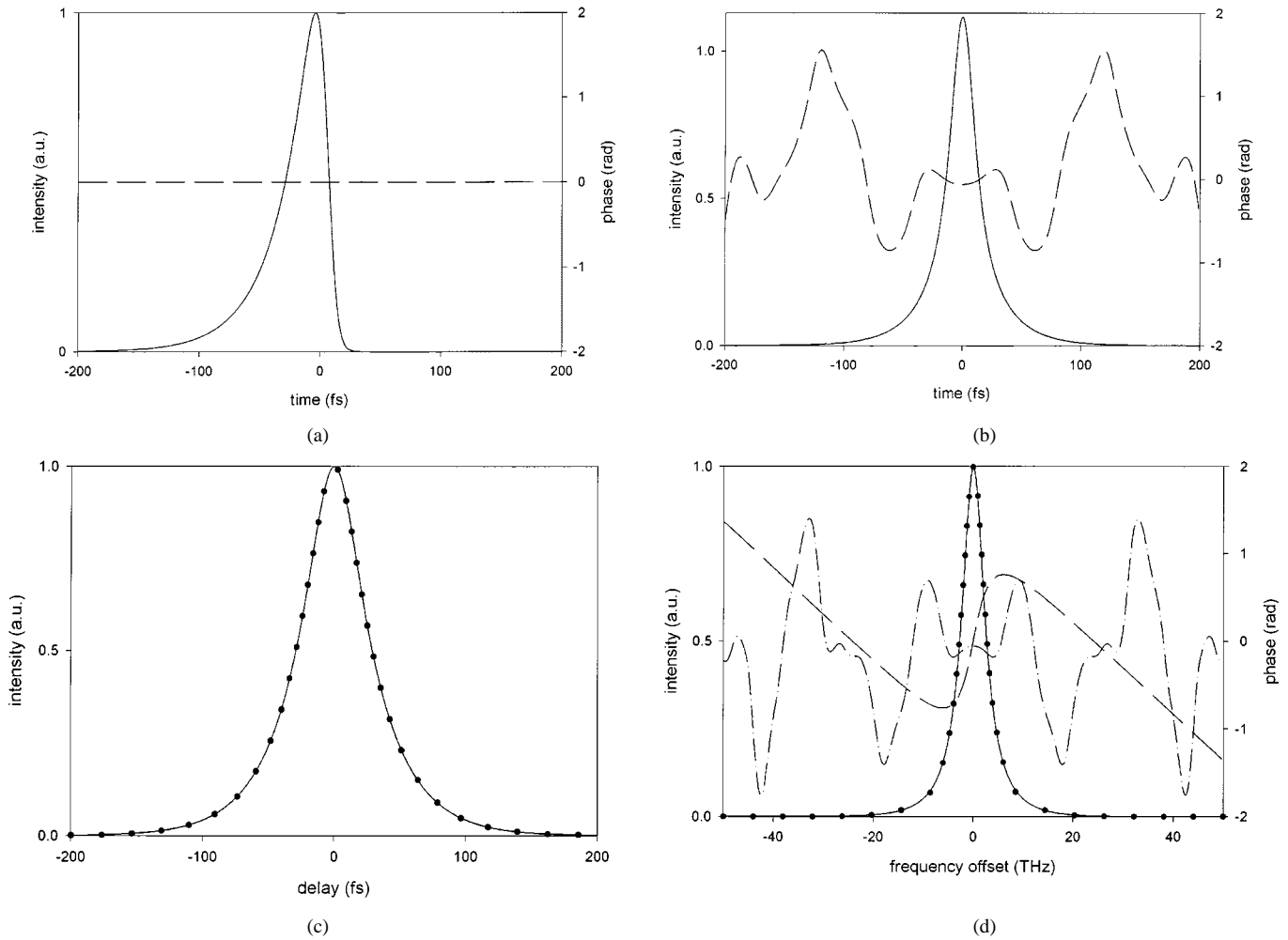
Fig. 2. Resultant traces in Example 1, where a pulse with small asymmetry and flat phase is assumed: The intensity (solid) and phase (dashed) of (a) asymmetric and (b) symmetric electric field envelopes. (c) Autocorrelation traces of the asymmetric (solid) and symmetric (dotted) pulses. (d) Power spectra of the asymmetric (solid) and symmetric (dotted) pulses and spectral phases of the same asymmetric (dashed) and symmetric (dashed–dotted) pulses.

They showed that those three data sets are sufficient for unique pulse reconstruction with time reversal the only remaining nontrivial ambiguity. In contrast, Peatross *et al.* [8] proposed a method to obtain the temporal intensity profile via temporal decorrelation of the (fringe-averaged) intensity autocorrelation function, using the nonnegativity condition for the temporal intensity. The result was combined with the power spectrum to retrieve the phase information via the Gerchberg–Saxton algorithm [9]. This approach was subsequently adapted in [10] for characterization of compressed pulses on the 5-fs time scale. A similar approach based on intensity autocorrelation and power spectrum data but with an improved reconstruction algorithm was subsequently published in [11]. Although these approaches [8], [10], [11] are still apparently utilized in practice, unlike Naganuma's algorithm they are based on only two one-dimensional data sets and have room for nontrivial ambiguities. Such ambiguities were mentioned in [8], which gave examples of nonunique pulse reconstructions for relatively complicated double-peaked pulses.

In this paper, we take a further look at ambiguities arising in pulse reconstruction using only the intensity autocorrelation and the power spectrum. In particular, we show how to construct pairs of distinct fields with identical or essentially identical in-

tensity autocorrelation and power spectrum traces. Our results show that even simple pulse shapes can be subject to severe ambiguities. We also compare the interferometric autocorrelation functions of the constructed field pairs. Although the interferometric autocorrelations are in fact distinct, as predicted by [7], the differences in the traces may be very small, which suggests that successful pulse retrieval using the method of [7] may be difficult in a practical context.

The ambiguity problem in phase retrieval has received considerable attention in various fields, such as microscopy, X-ray crystallography, and astronomy [12]–[20]. Many authors have dealt with the problem of reconstructing phase information of an object from a single data set, the modulus of its Fourier transform [12]–[19]. If the object is two-dimensional (a function of two variables, for example, x and y in space), the retrieved phase is unique both experimentally and theoretically in most practical cases [12]–[16].

The results are different for one-dimensional objects, which are functions of a single variable, such as x in space. Fienup illustrated that his algorithms using the modulus of the Fourier transform as the sole input generated severely ambiguous solutions [12]. One of these algorithms [14] was also adapted into the decorrelation process in [8] and [10]. Bruck *et al.* [13],

Fig. 3.   Resultant traces in Example 2, where a pulse with larger asymmetry and flat phase is assumed: The intensity (solid) and phase (dashed) of (a) asymmetric and (b) symmetric electric field envelopes. (c) Autocorrelation traces of the asymmetric (solid) and symmetric (dotted) pulses. (d) Power spectra of the asymmetric (solid) and symmetric (dotted) pulses and spectral phases of the same asymmetric (dashed) and symmetric (dashed–dotted) pulses.

Hayes [15], Walther [17], and Crimmins *et al.* [18], [19] all showed that in general, this one-dimensional phase reconstruction cannot have unique solutions without certain restrictions to the object to be characterized.

Closer to this paper's particular application, Huiser *et al.* proved that a one-dimensional function can be uniquely determined from its modulus and that of its Fourier transform [20]. In the case of femtosecond pulse reconstruction, this can be restated as the determination of the complete electric field profile from the square root of the temporal intensity profile and the square root of the power spectrum. Their proof was based on these assumptions: the function to be retrieved should have finite support and should be expressible in an analytic form (optically realizable in terms of microscopy). As they mentioned, however, the Gerchberg–Saxton algorithm may produce nonanalytic solutions that were excluded in their proof. Moreover, in the algorithm of [8], [10], and [11], the inputs are the power spectrum and the intensity autocorrelation (not the intensity itself, as postulated by Huiser *et al.* [20]). This increases the degree of ambiguity, which we illustrate by constructing very simple examples of distinct pulse pairs with identical or essentially identical power spectra and intensity autocorrelations.

The remainder of this paper is structured as follows. In Section II, we describe our approach after defining involved physical quantities. In Section III, we show several examples that illustrate ambiguity. In Section IV, we compare the interferometric autocorrelations of the constructed pulse pairs to assess the degree to which they can be distinguished in a practical context. We present conclusions in Section V.

II. DESCRIPTION OF OUR APPROACH

We first define our terminology. We write the electric field as

$$e(t) = \mathrm{Re}\left\{a(t)e^{j\omega_0 t}\right\} = \mathrm{Re}\left\{|a(t)|\, e^{j(\phi(t)+\omega_0 t)}\right\} \quad (1)$$

where
  $a(t)$ complex amplitude envelope function;
  $\phi(t)$ temporal phase function;
  ω_0 center angular frequency.
We assume that $a(t)$ is properly normalized so that the temporal intensity is given by

$$I(t) = |a(t)|^2. \quad (2)$$
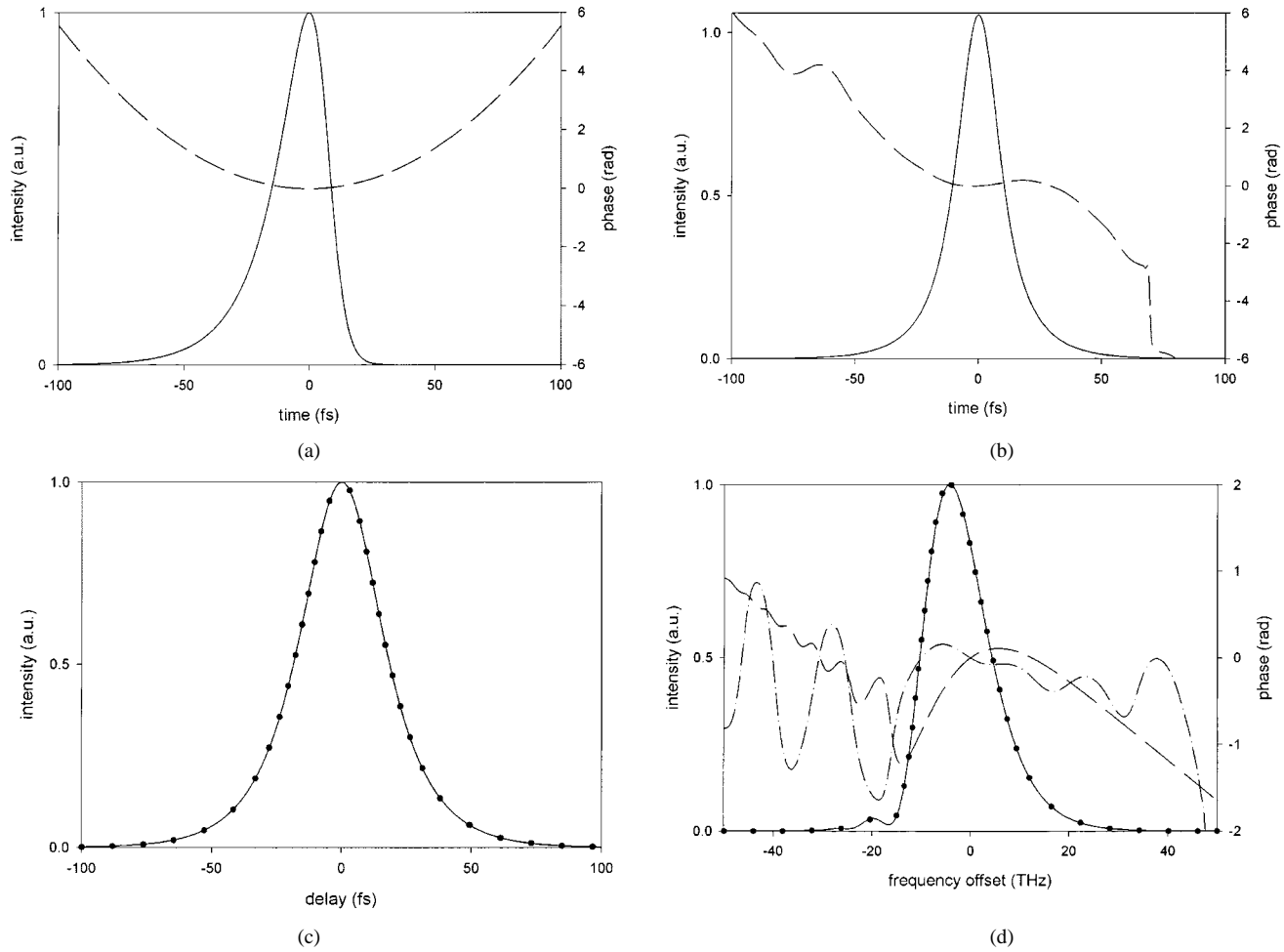
Fig. 4.   Resultant traces in the case of Example 3, where a pulse with small asymmetry and a quadratic temporal phase is assumed: The intensity (solid) and phase (dashed) of (a) the asymmetric and (b) symmetric electric field envelopes. (c) Autocorrelation traces of the asymmetric (solid) and symmetric (dotted) pulses. (d) Power spectra of the asymmetric (solid) and symmetric (dotted) pulses and spectral phases of the same asymmetric (dashed) and symmetric (dashed–dotted) pulses.

The Fourier transform of the electric field is written

$$\tilde{E}(\omega) = \frac{1}{2} \left\{ \tilde{A}(\omega - \omega_0) + \tilde{A}^*(-\omega - \omega_0) \right\} \qquad (3)$$

where $\tilde{A}(\omega)$ is the Fourier transform of $a(t)$. The actual power spectrum is expressed as

$$\left| \tilde{E}(\omega) \right|^2 = \frac{1}{4} \left\{ \left| \tilde{A}(\omega - \omega_0) \right|^2 + \left| \tilde{A}^*(-\omega - \omega_0) \right|^2 \right\}. \qquad (4)$$

However, in this paper, for the sake of convenience, we define the power spectrum $S(\omega)$ by its positive part shifted to the baseband, that is

$$S(\omega) = \left| \tilde{A}(\omega) \right|^2. \qquad (5)$$

Now let us consider autocorrelation measurements via second harmonic (SH) generation. We assume infinite phase-matching bandwidth for the second harmonic process [21]. Our discussion also applies to autocorrelation measurements obtained via two-photon absorption [22]. The measured time-averaged SH power has the form [7]

$$\int_{-\infty}^{\infty} P_{\mathrm{SHG}}(t)\, dt \propto 1 + 2G_2(\tau) + 4\mathrm{Re}\left\{ F_1(\tau) e^{j\omega_0\tau} \right\}$$

$$+ \mathrm{Re}\left\{ F_2(\tau) e^{2j\omega_0\tau} \right\} \qquad (6)$$

where

$$G_2(\tau) = \int_{-\infty}^{\infty} I(t) I(t - \tau)\, dt \qquad (7)$$

$$F_1(\tau) = \frac{1}{2} \int_{-\infty}^{\infty} \left\{ I(t) + I(t - \tau) \right\} a(t) a^*(t - \tau)\, dt \qquad (8)$$

$$F_2(\tau) = \int_{-\infty}^{\infty} \left\{ a(t) a^*(t - \tau) \right\}^2\, dt. \qquad (9)$$

The time-integrated SH power described in (6) is denoted as the interferometric autocorrelation, while the quantity varying slowly with the delay τ in (7) is the intensity autocorrelation function. The contribution from (9), which represents a term varying with frequency $2\omega_0$, is the SH field autocorrelation. The normal convention in plotting these quantities is to normalize the intensities such that

$$G_2(0) = \int_{-\infty}^{\infty} I^2(t)\, dt = 1. \qquad (10)$$

Let us now describe our approach. As in most algorithms and proofs, we assume that all the data sets have finite support in time, which is only approximately true for most ultrafast optical measurements. To meet this assumption, when we construct a pulse shape as a function of time, we use a time window very
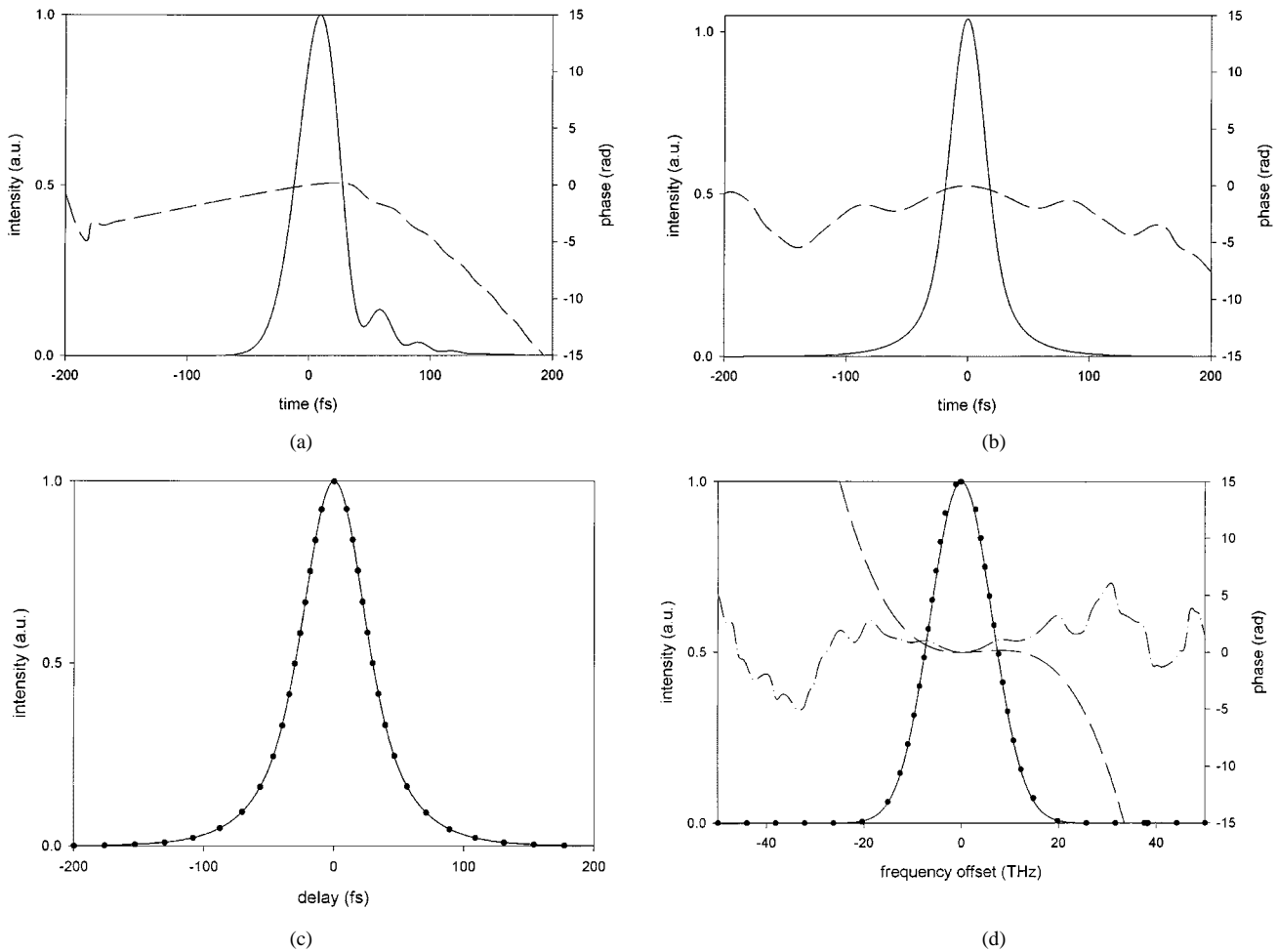
Fig. 5.   Resultant traces in the case of Example 4, where a Gaussian spectrum with a cubic and quadratic spectral phase is assumed: The intensity (solid) and phase (dashed) of (a) asymmetric and (b) symmetric electric field envelopes. (c) Autocorrelation traces of the asymmetric (solid) and symmetric (dotted) pulses. (d) Power spectra of the asymmetric (solid) and symmetric (dotted) pulses and spectral phases of the same asymmetric (dashed) and symmetric (dashed–dotted) pulses.

large compared to the pulsewidth, so that the field gets very close to zero on both sides. In the examples here, we represented each pulse with 1024 points with a 1-fs time interval between points, while the full-width at half-maximum (FWHM) of the longest pulse was 40 fs. In addition, two finite-supported data sets are assumed to be available by measurements: the intensity autocorrelation $G_2(\tau)$ and the power spectrum $S(\omega)$. We then usually go through the following steps to construct pairs of distinct fields with the same $G_2(\tau)$ and $S(\omega)$.

1) We first choose an asymmetric intensity profile $I_a(t)$ and then generate its autocorrelation $G_2(\tau)$.
2) The Fourier transform of $G_2(\tau)$ gives $|\tilde{I}_a(\omega)|^2$, where $\tilde{I}_a(\omega)$ is the Fourier transform of $I_a(t)$. By setting the spectral phase of $\tilde{I}_a(\omega)$ to zero, we can derive a new function $\tilde{I}_s(\omega) = |\tilde{I}_a(\omega)|$ with an autocorrelation identical to that of the original asymmetric intensity profile but corresponding to a symmetric intensity profile $I_s(t)$.
3) We then assign a specific temporal phase to either the asymmetric or the symmetric temporal field envelope and Fourier-transform it to find the resulting power spectrum $S(\omega)$. The temporal phase of one of the field envelopes is left unspecified at this point.

4) Finally, we apply Gerchberg–Saxton's method [9] to retrieve a temporal phase profile for the pulse left unspecified in Step 3), using both the previously specified intensity profile and power spectrum $S(\omega)$ as constraints.

This approach results in a pair of pulses, one symmetric and one asymmetric, with identical intensity autocorrelations and identical or essentially identical power spectra.

In the following, we will present numerical results based on two different minor variations of this procedure.

- In the first case (Case I), the temporal phase of the asymmetric pulse is specified in Step 3), while that of the symmetric pulse is found via the iterative algorithm. This procedure is illustrated schematically in Fig. 1 and is used for the results shown in Figs. 2–4.
- In Case II, which is very similar to Case I, we specify the initial asymmetric pulse in the frequency domain—i.e., we specify $\tilde{A}_a(\omega)$ for the asymmetric pulse, including its spectral phase, whose square gives the power spectrum. We then inverse Fourier transform to obtain both the intensity profile $I_a(t)$ of the asymmetric pulse and its corresponding phase $\phi_a(t)$ at the same time. We then follow Steps 1), 2), and 4) of our procedure, omitting Step 3),

TABLE I
CONSTANTS USED TO GENERATE INITIAL ASYMMETRIC PULSE SHAPES IN EXAMPLES 1–3

Example	Figure	t_p (fs)	a	b	$\phi_a(t)$ (rad)	$\phi_s(t)$ (rad)
1	2	40	7	1.4	0	Unspecified
2	3	40	7	0.7	0	Unspecified
3	4	40	7	1.4	$(5.6 \times 10^{26})t^2$	Unspecified

TABLE II
PULSEWIDTHS OF THE FOUR EXAMPLES

(Unit: fs)

Example	Pulse shape	Full Width at Half Maximum	Power-Equivalent Width	Root Mean Square Width	Full Width at 10%-maximum	Full Width at 1%-maximum
1	Asymmetric	23.9	28.4	31.5	54.0	94.2
	Symmetric	21.2	26.9	31.5	53.0	107.7
2	Asymmetric	36.6	45.4	59.0	90.2	163.6
	Symmetric	28.3	40.7	59.0	87.2	196.3
3	Asymmetric	23.9	28.4	31.5	54.0	94.2
	Symmetric	21.2	26.9	31.5	53.0	107.7
4	Asymmetric	40.0	47.1	53.9	98.9	177.0
	Symmetric	36.8	45.2	53.9	83.7	187.5

which is already accomplished. This case is illustrated by Fig. 5.

We also tried the converse of Case I—namely, the temporal phase of the symmetric pulse is specified in Step 3), while the phase of asymmetric pulse is found via phase retrieval. To get good convergence, we found that an additional least squares optimization step was needed after the Gerchberg–Saxton algorithm. Furthermore, the resulting symmetric–asymmetric pulse pairs that we obtained were less distinct than in the other cases we considered. Therefore, we will not discuss this case further.

III. RECONSTRUCTION RESULTS

We present four examples, which are shown in Figs. 2–5. For the first three examples, the initial asymmetric pulses are taken to have the form

$$I_a(t) \propto \frac{1}{\{\exp(at/t_p) + \exp(-bt/t_p)\}^2} \tag{11}$$

where t_p, a, and b are listed in Table I. In regard to the phase profiles, for the first two examples a flat temporal phase was assigned to each initial asymmetric pulse, while in the third example a quadratic phase was chosen for the asymmetric pulse. These are also enumerated in Table I. In the fourth example, corresponding to Case II of our algorithm, the initial pulse was constructed in the frequency domain and corresponds to a pulse with Gaussian spectral amplitude and quadratic and cubic spectral phase.

Fig. 2 shows the result of Example 1, the case when the initially assumed pulse has relatively small asymmetry and flat phase [Fig. 2(a)]. After running the Gerchberg–Saxton algorithm, we obtain the phase of the symmetric electric field envelop shown in Fig. 2(b), which has distinctly different intensity and phase profiles from those in Fig. 2(a). The FWHM of the asymmetric pulse is 23.9 fs, while that of the symmetric pulse is 21.2 fs. Other pulsewidths defined in different ways, listed in Table II, show more clearly the disparity between the two

pulses. The intensity autocorrelations of the asymmetric–symmetric pair are shown in Fig. 2(c) and are not distinguishable. Fig. 2(d) also illustrates the two power spectra that are nearly identical but with two different spectral phase profiles. The very small difference between the two power spectra (visible only on a log plot) is believed to be limited by the stagnation of the iterative algorithm but requires a further investigation. Regardless of what causes the error, however, in a practical context such a subtle difference can be easily overwhelmed by noise or measurement inaccuracies so that the two power spectra can be considered as identical. Log-scaled plots of the power spectra will be shown after all examples are introduced.

This error was observed in the power spectrum and not in the temporal intensity profile because the temporal intensity profile constraint was applied as the final step prior to halting the Gerchberg–Saxton algorithm when the stagnation occurred. To quantify this difference, we define an rms error in the power spectra by

$$\varepsilon_S = \left(\frac{1}{N} \sum_{k=1}^{N} |S_a(\omega_k) - S_s(\omega_k)|^2 \right)^{1/2} \tag{12}$$

where N is the number of points in the frequency domain, for which each power spectrum has significant nonzero values—i.e., values larger than 10^{-6} maximum, ω_k, $k = 1, 2, \ldots, N$ is the angular frequency at each point, and $S_a(\omega)$ and $S_s(\omega)$ are the asymmetric and symmetric power spectrum, respectively, which are normalized so that their maximum values are unity. According to this definition, the error between two power spectra was $\varepsilon_S = 1.7 \times 10^{-3}$ in this example. This error is sufficiently low that these data constitute strong evidence of the ambiguity of pulse reconstruction based only on $G_2(\tau)$ and $S(\omega)$.

Fig. 3 shows the traces resulting from Example 2, which is similar to Example 1 except with larger asymmetry in the initial pulse intensity [Fig. 3(a)]. We can very clearly differentiate
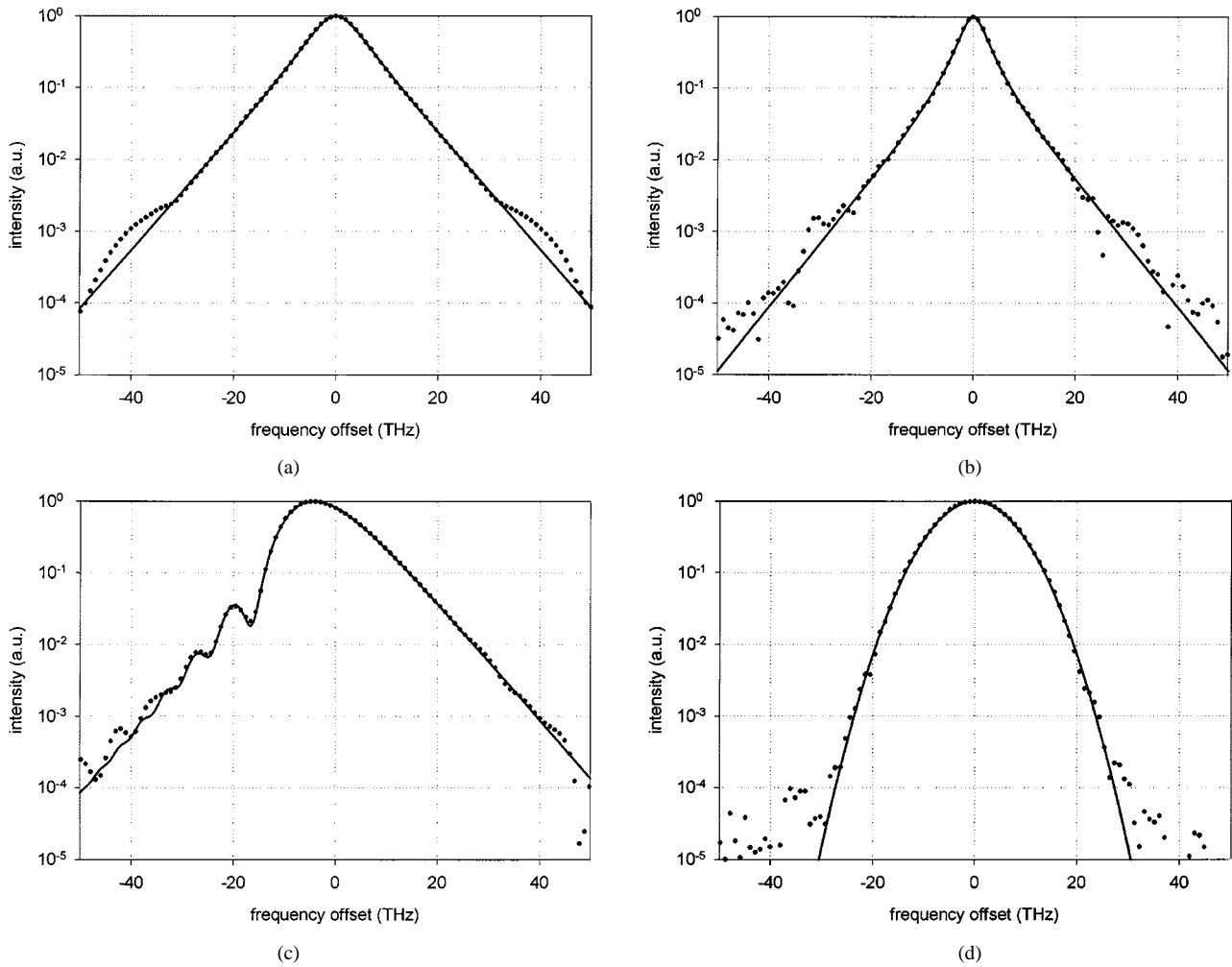
Fig. 6.   Log-scaled power spectra of (a) Example 1, (b) Example 2, (c) Example 3, and (d) Example 4. Asymmetric pulse: solid; symmetric pulse: dotted.

the symmetric intensity profile in Fig. 3(b) from the asymmetric profile, which is also indicated by pulsewidths in Table II. For example, the FWHM of the asymmetric pulse is 36.6 fs, while that of the symmetric pulse is 28.3 fs. The difference between them is 8.3 fs, which is larger than that in Example 1, 2.7 fs. The fact that those two have identical autocorrelations and essentially identical power spectra is also verified from Fig. 3(c) and (d). The reconstruction error in the power spectra was $\varepsilon_S = 7.3 \times 10^{-4}$.

Example 3 uses the same input $I_a(t)$ as in Example 1, but with a quadratic phase assigned to the asymmetric pulse shape, i.e., $\phi_a(t) = (5.6 \times 10^{26})t^2$ with t in seconds, as shown in Fig. 4(a). Our algorithm again produces a good result, a totally new symmetric pulse amplitude and phase [Fig. 4(b)] but with identical autocorrelations and essentially identical power spectra, shown in Fig. 4(c) and (d), respectively. The temporal phase $\phi_s(t)$ of the symmetric pulse is clearly very different from a quadratic and is instead more similar to a cubic in the main part of the pulse. All the pulsewidths for this pair, listed in Table II, are identical to those of Example 1, which also supports the accuracy of our reconstruction algorithm. We note that unlike the previous two examples, an asymmetric power spectrum results from the chirped asymmetric input pulse. The error in the power spectra was $\varepsilon_S = 2.2 \times 10^{-3}$.

Lastly, Example 4 is obtained through Case II, where we assume a Gaussian spectrum with quadratic and cubic phase. Specifically, the spectral amplitude of the asymmetric pulse was given by

$$\tilde{A}_a(\omega) = \exp(-t_p^2 \omega^2/4) \exp\left[j \left\{ -(\omega/a)^3 + (\omega/b)^2 \right\} \right] \quad (13)$$

where $t_p = 25$ fs, $a = 72.9 \times 10^{12}$ rad/s, and $b = 70.2 \times 10^{12}$ rad/s. This gives the initial asymmetric temporal pulse illustrated in Fig. 5(a). The same iterative algorithm as in the previous examples generates the phase of the symmetric pulse as shown in Fig. 5(b). Their FWHMs are 40.0 fs for the asymmetric and 36.8 fs for the symmetric pulse, as listed in Table II. Their autocorrelations and power spectra are illustrated in Fig. 5(c) and (d), respectively. Again the former are indistinguishable, while the power spectra have a slight error of $\varepsilon_S = 8.2 \times 10^{-3}$. The symmetric pulse shows no sign of a cubic spectral phase.

In Fig. 6, we show log-scaled plots of the power spectra in the foregoing four examples in order to clarify the differences that they have. We can observe that the errors in all examples occur only below the 0.002 level. Without extremely accurate measurements, these errors cannot be detected and the pairs of power spectra are practically identical.

In Table II, we compare the four pulse pairs presented in this section in terms of the pulsewidth. We calculated intensity full
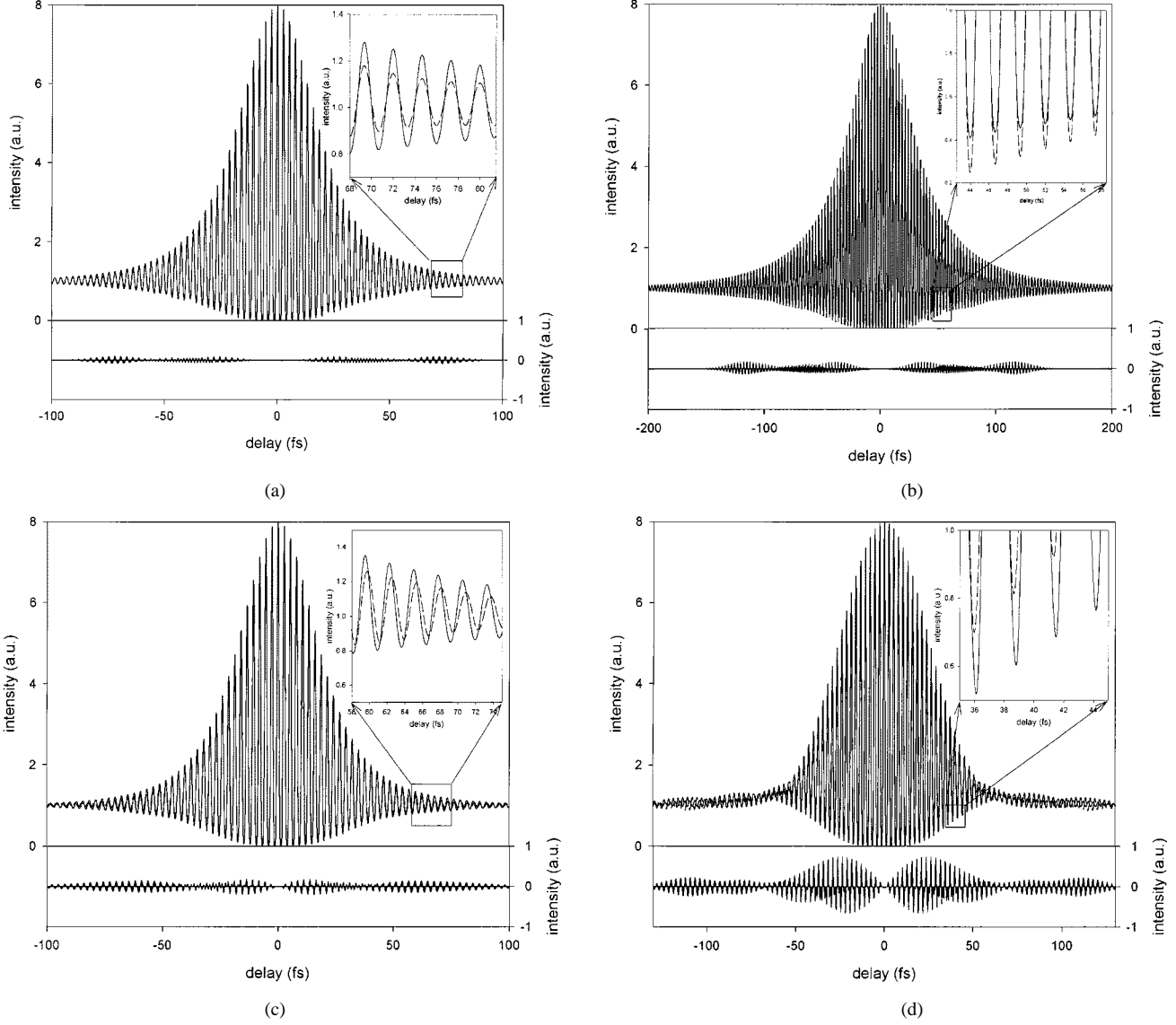
Fig. 7. The interferometric autocorrelations for the asymmetric (solid) and symmetric (dashed) pulse pair corresponding to (a) Example 1, (b) Example 2, (c) Example 3, and (d) Example 4. Each inset magnifies the region with the large difference (asymmetric pulse: solid; symmetric pulse: dashed). Each bar graph at the bottom shows the difference of the asymmetric IAC to the symmetric IAC.

widths at half-maximum, 10% maximum, and 1% maximum, power-equivalent pulsewidth, and rms pulsewidth. The power-equivalent pulsewidth is the pulse energy divided by the peak pulse power [23], that is

$$\tau_{\text{PEW}} = \frac{\int_{-\infty}^{\infty} I(t)\, dt}{\max\left(I(t)\right)} \quad (14)$$

and the rms pulsewidth is defined by [24]

$$\tau_{\text{rms}} = 2\sqrt{\langle t^2 \rangle - \langle t \rangle^2} \quad (15)$$

where

$$\langle f(t) \rangle = \frac{\int_{-\infty}^{\infty} f(t) I(t)\, dt}{\int_{-\infty}^{\infty} I(t)\, dt}. \quad (16)$$

The rms width is a good measure for the accuracy of our algorithm because it is a quantity that can be derived directly from the intensity autocorrelation without the knowledge of the pulse shape [24]. Table II shows that for all the pairs the two rms widths are identical to each other, which is further evidence of the validity of our approach. Since in each example the difference of the full width is larger at lower intensity levels, we can see most clearly the disparity of the two pulses at 1% maximum. As mentioned in the above, the data of Examples and 3 are identical because the pulsewidths depend only on Steps 1) and 2), for which they are identical, unless the algorithm changes the input intensity profile. Also it is interesting to note that among the four columns excluding the rms width, the width of symmetric pulse exceeds that of the asymmetric pulse only in the full width at 1% maximum.

IV. COMPARISON OF INTERFEROMETRIC AUTOCORRELATIONS

As mentioned in Section I, Naganuma *et al.* proposed an algorithm to uniquely retrieve a pulse shape from the elec-

tric field autocorrelation and the interferometric autocorrelation (IAC) measurements with time reversal as the only nontrivial ambiguity [7]. The intensity autocorrelation and the SH field autocorrelation are extracted from the IAC trace through low-pass filtering and bandpass filtering at the SH frequency, respectively. In real experiments, however, the measured IAC is subject to noise and other measurement errors. Therefore, the information needed to distinguish between two different pulses with identical electric field autocorrelations (equivalently, power spectra) may be masked in cases where the two IACs differ only slightly.

To explore this issue further, we have generated the IACs for each of the asymmetric–symmetric pulse pairs in the four examples. Our results are illustrated in Fig. 7. In every case we assume that the center wavelength is 800 nm and use a 0.05-fs delay increment. Each inset shows in detail a region where the two IACs have the most visible difference. Each bar graph at the bottom represents the difference between them—i.e., the IAC of the asymmetric pulse subtracted by that of the symmetric pulse. We can again define the rms error ε_{IAC} in these autocorrelations using (12) with $S(\omega)$ replaced by the normalized IAC. The number of points in the delay axis is fixed to 8000 in all IACs. Then the rms errors are $\varepsilon_{IAC} = 3.4\times 10^{-3}$ for Example 1 [Fig. 7(a)], $\varepsilon_{IAC} = 7.1\times 10^{-3}$ for Example 2 [Fig. 7(b)], $\varepsilon_{IAC} = 7.0\times 10^{-3}$ for Example 3 [Fig. 7(c)], and $\varepsilon_{IAC} = 2.2\times 10^{-2}$ for Example 4 [Fig. 7(d)]. Another measure for comparison is the ratio of the maximum difference to the maximum value of the IAC, which is 1.3% for Example 1, 2.3% for Example 2, 2.6% for Eexample 3, and 9.3% for Example 4. These values can be observed from the bottom bar graphs. We note that for each symmetric–asymmetric pulse pair, the IACs are in fact distinct, as predicted by Naganuma [7]. However, except for Example 4, the differences in the IACs are very subtle.

We first compare the two nonchirped cases, Examples 1 and 2. Remembering that the only difference between them is the degree of asymmetry, we can infer that as the asymmetry gets smaller, the corresponding IACs resemble each other more closely. Moreover, their fringes remain in phase even at the far wings, which will make the discrimination between symmetric and asymmetric pulses more difficult. The IACs of Example 3 [Fig. 7(c)], where a quadratic temporal phase was assumed, show a difference comparable to that of Example 2, even though the degree of asymmetry is as small as in Example 1. The chirp also generates a difference in the phase of the fringes in the far wings. However, in the case where the chirp is not so strong, these differences are weak. On the other hand, as shown in Fig. 7(d), the cubic spectral phase component of the asymmetric pulse leads to a greater distinction between its IAC and that of the symmetric pulse. The relatively large difference near the center of the traces, together with the out-of-phase oscillations in the wings, should be enough to distinguish these traces experimentally.

Since the intensity and SH field autocorrelations are derived by filtering the IAC in the frequency domain, we take a look at the Fourier transform of the IAC. Fig. 8 shows the power spectra of the two IACs corresponding to Examples 1 [Fig. 8(a)] and 4 [Fig. 8(b)]. Because the IAC is a real and even
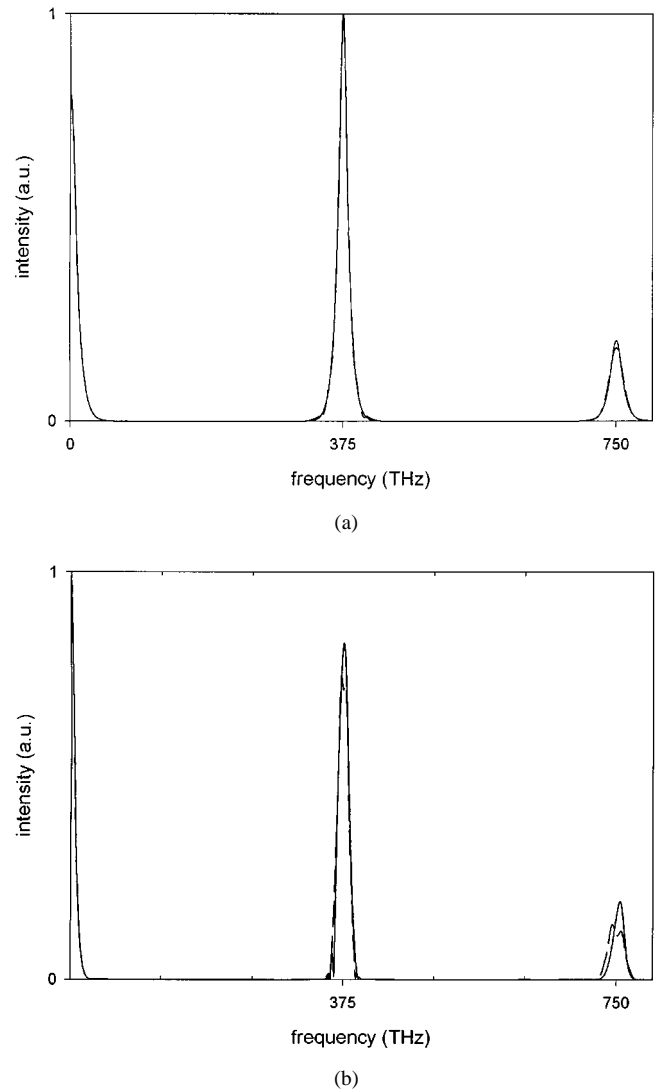

(a)

(b)

Fig. 8. Power spectra of the IACs corresponding to (a) Example 1 and (b) Example 4 (asymmetric pulse: solid; symmetric pulse: dashed).

quantity, its Fourier transform is real, and therefore the power spectrum retains full information. Similar to the corresponding IACs, Fig. 8(a) shows only a very subtle difference between the two traces while Fig. 8(b) shows a more noticeable disparity. In Fig. 8(a), the slight difference occurs mostly at the SH frequency $2\omega_0$. On the other hand, in Fig. 8(b) we can observe differences located around both the center frequency ω_0 and the SH frequency. Also in Fig. 8(b), both the ω_0 and $2\omega_0$ peaks in the IAC power spectrum of the symmetric pulse are slightly red-shifted compared to those for the asymmetric pulse. These shifts are related to the out-of-phase oscillations observed in the wings of the IACs in time domain.

From these observations, we submit that in a practical context, where signal-to-noise ratio (SNR) and measurement accuracy are not perfect, it may not be possible to distinguish between certain quite distinct waveforms from their IACs. Under these circumstances, pulse reconstruction algorithms based on the IAC may fail to retrieve the correct result. Examples 1 to 3 considered above are illustrations of the cases where such reconstruction may fail unless the measurement data are of extremely high quality.
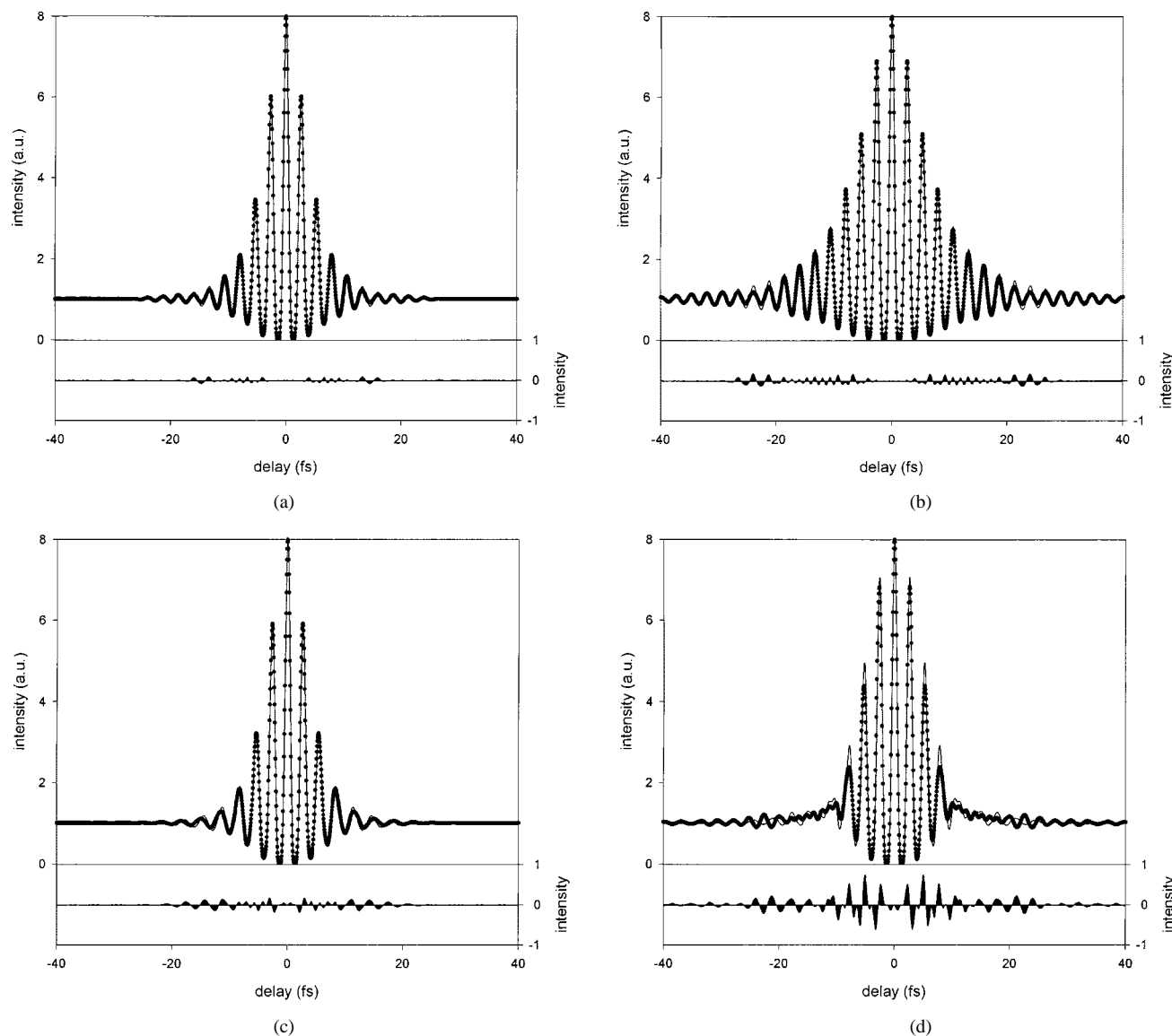
Fig. 9. The IACs of sub-10-fs pulse pairs corresponding to (a) Example 1, (b) Example 2, (c) Example 3, and (d) Example 4. (Asymmetric pulse: solid; symmetric pulse: circle.) Each bar graph at the bottom shows the difference of the asymmetric IAC to the symmetric IAC.

Finally, let us comment on the IACs in the context of measurement of sub-10-fs pulses. Although FROG and SPIDER measurements can indeed be performed in this regime [25], [26], many researchers still rely primarily on comparison of the experimental IAC with the theoretical IAC based on the power spectrum supplemented by an assumed spectral phase. To address this point, we took the electric field profiles from Fig. 7 and rescaled the time axis by a factor of five. This results in a series of pulses with sub-10-fs pulse durations. The IACs were then recalculated and plotted in Fig. 9. Fig. 9(a)–(d) corresponds to Examples 1–4, respectively. In all cases except Example 4, it is difficult to distinguish the IAC corresponding to the symmetric pulse to that of the asymmetric pulse, even though, as we have seen, the two pulses have quite distinct characteristics. Moreover, the slight differences in the IACs occur mainly in the wings and not in the central region. This implies that matching the measured IAC and the calculated IAC only in the central region can give only a rough estimate of the pulse duration. At a minimum,

matching the IACs extremely carefully in the wings as well as in the center appears to be necessary to yield further information.

V. CONCLUSION

We have investigated the ambiguity of the retrieval methods based only on the use of the optical power spectrum and intensity autocorrelation. We have described an approach to construct a pair of asymmetric and symmetric pulses with identical or essentially identical power spectra and intensity autocorrelations. We also presented four examples showing that the two pulses have quite different phase and temporal amplitude profiles. In one case, the difference in the FWHM pulse durations was on the order of 25%. These results elucidate the ambiguity inherent in reconstruction based on the power spectrum and the intensity autocorrelation.

Furthermore, we used these symmetric–asymmetric pulse pairs as test cases to assess the degree of difference in the corresponding IAC pairs. In the three cases, we found that the resulting

IAC pairs are sufficiently similar that they might be quite challenging to distinguish in a practical experimental context. These findings illustrate that in some cases, IAC data may be only very weakly sensitive to rather significant changes in pulse shape.

ACKNOWLEDGMENT

REFERENCES

[1] R. Trebino, K. W. DeLong, D. N. Fittinghoff, J. N. Sweetser, M. A. Krumbugel, and B. A. Richman, "Measuring ultrashort laser pulses in the time-frequency domain using frequency-resolved optical gating," *Rev. Sci. Instrum.*, vol. 68, pp. 3277–3295, 1997.

[2] C. Iaconis and I. A. Walmsley, "Self-referencing spectral interferometry for measuring ultrashort optical pulses," *IEEE J. Quantum Electron.*, vol. 35, pp. 501–509, 1999.

[3] J. K. Rhee, T. S. Sosnowski, A. C. Tien, and T. B. Norris, "Real-time dispersion analyzer of femtosecond laser pulses with use of a spectrally and temporally resolved upconversion technique," *J. Opt. Soc. Amer. B*, vol. 13, pp. 1780–1785, 1996.

[4] K. C. Chu, J. P. Heritage, R. S. Grant, K. X. Liu, A. Dienes, W. E. White, and A. Sullivan, "Direct measurement of the spectral phase of femtosecond pulses," *Opt. Lett.*, vol. 20, pp. 904–906, 1995.

[5] E. P. Ippen and C. V. Shank, "Techniques for measurement," in *Ultrashort Light Pulses: Picosecond Techniques and Applications*, S. L. Shapiro, Ed. Berlin, Germany: Springer, 1977.

[6] J.-C. Diels and W. Rudolph, *Ultrashort Laser Pulse Phenomena: Fundamentals, Techniques, and Applications on a Femtosecond Time Scale*. San Diego, CA: Academic, 1996, ch. 8.

[7] K. Naganuma, K. Mogi, and J. Yamada, "General method for ultrashort light pulse chirp measurement," *IEEE J. Quantum Electron.*, vol. 25, pp. 1225–1233, 1989.

[8] J. Peatross and A. Rundquist, "Temporal decorrelation of short laser pulses," *J. Opt. Soc. Amer. B*, vol. 15, pp. 216–222, 1998.

[9] R. W. Gerchberg and W. O. Saxton, "A practical algorithm for the determination of phase from image and diffraction plane pictures," *Optik*, vol. 35, pp. 237–246, 1972.

[10] A. Baltuska, Z. Wei, M. S. Pshenichnikov, D. A. Wiersma, and R. Szipocs, "All-solid-state cavity-dumped sub-5-fs laser," *Appl. Phys. B*, vol. 65, pp. 175–188, 1997.

[11] A. Baltuska, A. Pugzlys, M. S. Pshenichnikov, and D. A. Wiersma, "Rapid amplitude-phase reconstruction of femtosecond pulses from intensity autocorrelation and spectrum," in *Conf. Lasers and Electro-optics (CLEO)*, Baltimore, MD, May 23–28, 1999.

[12] J. R. Fienup, "Reconstruction of an object from the modulus of its Fourier transform," *Opt. Lett.*, vol. 3, pp. 27–29, 1978.

[13] Y. M. Bruck and L. G. Sodin, "On the ambiguity of the image reconstruction problem," *Opt. Commun.*, vol. 30, pp. 304–308, 1979.

[14] J. R. Fienup, "Phase retrieval algorithms: A comparison," *Appl. Opt.*, vol. 21, pp. 2758–2769, 1982.

[15] M. H. Hayes, "The unique reconstruction of multidimensional sequences from Fourier transform magnitude or phase," in *Image Recovery: Theory and Application*, H. Stark, Ed. Orlando, FL: Academic, 1987.

[16] R. P. Millane, "Phase retrieval in crystallography and optics," *J. Opt. Soc. Amer. A*, vol. 7, pp. 394–411, 1990.

[17] A. Walther, "The question of phase retrieval in optics," *Opt. Acta*, vol. 10, pp. 41–49, 1963.

[18] T. R. Crimmins and J. R. Fienup, "Ambiguity of phase retrieval for functions with disconnected support," *J. Opt. Soc. Amer.*, vol. 71, pp. 1026–1028, 1981.

[19] ——, "Uniqueness of phase retrieval for functions with sufficiently disconnected support," *J. Opt. Soc. Amer.*, vol. 73, pp. 218–221, 1983.

[20] A. M. J. Huiser, A. J. J. Drenth, and H. A. Ferwerda, "On phase retrieval in electron microscopy from image and diffraction pattern," *Optik*, vol. 45, pp. 303–316, 1976.

[21] A. M. Weiner, "Effect of group velocity mismatch on the measurement of ultrashort optical pulses via second harmonic generation," *IEEE J. Quantum Electron.*, vol. QE-19, pp. 1276–1283, 1983.

[22] J. K. Ranka, A. L. Gaeta, A. Baltuska, M. S. Pshenichnikov, and D. A. Wiersma, "Autocorrelation measurement of 6-fs pulses based on the two-photon-induced photocurrent in a GaAsP photodiode," *Opt. Lett.*, vol. 22, pp. 1344–1346, 1997.

[23] B. E. A. Saleh and M. C. Teich, *Fundamentals of Photonics*. New York: Wiley, 1991.

[24] E. Sorokin, G. Tempea, and T. Brabec, "Measurement of the root-mean-square width and the root-mean-square chirp in ultrafast optics," *J. Opt. Soc. Amer. B*, vol. 17, pp. 146–150, 2000.

[25] G. Taft, A. Rundquist, M. M. Murnane, I. P. Christov, H. C. Kapteyn, K. W. DeLong, D. N. Fittinghoff, M. A. Krumbugel, J. N. Sweetser, and R. Trebino, "Measurement of 10-fs laser pulses," *IEEE J. Select. Topics Quantum Electron.*, vol. 2, pp. 575–585, 1996.

[26] L. Gallmann, D. H. Sutter, N. Matuschek, G. Steinmeyer, U. Keller, C. Iaconis, and I. A. Walmsley, "Characterization of sub-6-fs optical pulses with spectral phase interferometry for direct electric-field reconstruction," *Opt. Lett.*, vol. 24, pp. 1314–1316, 1999.

Jung-Ho Chung (S'01) received the B.S. degree in electrical engineering from Seoul National University, Seoul, Korea, in 1997, and the M.S. degree in electrical and computer engineering from Purdue University, West Lafayette, IN, where he is currently pursuing the Ph.D. degree in electrical engineering.

Until 1999, he worked on code-division multiple-access communication systems at Korea Telecom Freetel, Seoul, Korea. He is doing research in the Ultrafast Optics and Optical Fiber Communications Laboratory on space-time processing of ultrafast optical pulses, as well as on ambiguity problems of pulse retrieval.

Andrew M. Weiner (S'84–M'84–SM'91–F'95) was born in Boston, MA, in 1958. He received the Sc.D. degree in electrical engineering from the Massachusetts Institute of Technology (MIT), Cambridge, in 1984.

From 1979 through 1984, he was a Fannie and John Hertz Foundation Graduate Fellow at MIT. His doctoral thesis dealt with femtosecond pulse compression (including generation of the shortest optical pulses reported up to that time) and measurement of femtosecond dephasing in condensed matter. In 1984, he joined Bellcore, where he conducted research on ultrafast optics, including shaping of ultrashort pulses, nonlinear optics and switching in fibers, and spectral holography. In 1989, he became Manager of the Ultrafast Optics and Optical Signal Processing Research District. He joined Purdue University as a Professor of electrical and computer engineering in 1992. Since 1996, he has also been Director of Graduate Admissions for the School of Electrical and Computer Engineering. He spent the 1999–2000 academic year as a Visiting Professor at the Max Born Institute for Nonlinear Optics and Short Pulse Spectroscopy in Berlin, Germany. His current research interests center on processing of ultrashort pulses, high-speed optical communications, applications of pulse shaping to femtosecond spectroscopy and nonlinear optics, terahertz radiation, and optical imaging in scattering media. He has published four book chapters and approximately 100 journal articles. He is author or coauthor of 200 conference papers, including approximately 60 conference invited talks, and has presented more than 50 additional invited seminars at universities or industry. He has received five U.S. patents. He has served on or chaired numerous research review panels, professional society award committees, and conference program committees. He was General Co-Chair of the 1998 Conference on Lasers and Electro-optics and Chair of the 1999 Gordon Conference on Nonlinear Optics and Lasers. He was Associate Editor of *Optics Letters*.

Prof. Weiner is a Fellow of the Optical Society of America. He received the 1984 Hertz Foundation Doctoral Thesis Prize. In 1988–1989, he was selected as an IEEE Lasers and Electro-optics Society (LEOS) Traveling Lecturer. In addition, he was Associate Editor for the IEEE JOURNAL OF QUANTUM ELECTRONICS and IEEE PHOTONICS TECHNOLOGY LETTERS. He received the 1990 Adolph Lomb Medal from the Optical Society of America for pioneering contributions to the field of optics made before the age of 30. He received the Curtis McGraw Research Award of the American Society of Engineering Education (1997), the International Commission on Optics Prize (1997), the IEEE LEOS William Streifer Scientific Achievement Award (1999), and the Alexander von Humboldt Foundation Research Award for Senior U.S. Scientists (2000). He was an elected Member of the Board of Governors of the IEEE Lasers and Electro-optics Society from 1997 to 1999 and is currently Secretary/Treasurer of that organization.